ARTICLE

Journal of Materials Chemistry
www.rsc.org/materials

An investigation of the structure of stearate monolayers on $Au@ZrO_2$ and $Ag@ZrO_2$ core–shell nanoparticles†

A. Sreekumaran Nair,[a] T. Pradeep*[a] and I. MacLaren[b]

[a]*Department of Chemistry and Sophisticated Analytical Instrumentation Facility, Indian Institute of Technology Madras, Chennai 600 036, India. E-mail: pradeep@iitm.ac.in*
[b]*Institute for Materials Science, Darmstadt University of Technology, 64287 Darmstadt, Germany*

Received 31st October 2003, Accepted 18th December 2003
First published as an Advance Article on the web 30th January 2004

Monolayer protected nanoparticles, $Au@ZrO_2$@stearate and $Ag@ZrO_2$@stearate, in which the core–shell nanoparticles, $Au@ZrO_2$ and $Ag@ZrO_2$ (ZrO_2 coated Au and Ag nanoparticles) are functionalized with stearic acid, have been synthesized and characterized. The air-dried powders, freely dispersible in several organic solvents (both polar and non-polar), are stable for extended periods. The materials were characterized by spectroscopic, microscopic, diffraction and thermal analysis techniques. The monolayer cover is stable up to 200 °C. Monolayers do not exhibit strong inter-chain interactions, unlike in the case of those on metal nanoparticles, suggesting that their surface anchoring sites are widely spaced. As a result, temperature-dependent infrared spectra of the monolayers are featureless. The oxide surface is accessible for small molecules in solution even after stearic acid coverage. Freely dispersible nanoparticles with oxide shells may offer new possibilities in catalysis, photophysics and materials science.

Introduction

Nanomaterials research is a rapidly expanding field and has opened up exciting possibilities for these materials in electronic, magnetic, catalytic and electrochemical applications.[1] Core–shell nanoparticles are part of the recent development in this area, monolayer-protected clusters[1e] themselves can be considered as core–shell materials.[2] Such materials have unique and well-defined properties, which are tunable depending on the nature of the metal, the size and shape of the core and the nature of the monolayer chosen.[3] Oxide covered noble metal clusters have been synthesized by several groups;[4,5] we have recently reported the synthesis, characterization and properties of $Au@ZrO_2$ and $Ag@ZrO_2$ core–shell materials.[5] The core–shell geometry helps in the control of inter-particle interactions contributing to the functional properties of devices; and as a result, the range of potential applications expands.[4c] This geometry also allows for the enhancement in the luminescence of semiconductor nanoparticles,[6] aids in the preparation of bioconjugates,[7,8] increases colloidal stability,[9] enables the preparation of charged metal cores,[10] and helps in the optimization of electrical and magnetic properties.[11] Core–shell structures with oxides forming both core and shell have been investigated by Vollath *et al.*[12] The possibilities for core–shell nanoparticles in photonics have been recently demonstrated by Blaaderen *et al.*[13] The porosity of the shell is an important aspect, which has been investigated recently by the present authors. The existence of pores permits selective entry of molecules such as halocarbons through the shell thereby making the reaction between the metal core and halogens possible, creating metal oxide nanobubbles.[14] Recently, the synthesis and characterization of $Au@SiO_2$ core–shell nanoparticles incorporating a mercaptosilane at the core–shell interface has been reported by Katz *et al.*[15]

Core–shell particles, especially the oxide covered ones, have a major limitation, as they are prone to aggregation. As a result, purification of these materials is difficult. One approach towards overcoming this problem is functionalizing the shell using monolayers of suitable molecules with the principal aim of achieving re-dispersibility. With suitable monolayer-forming molecules, these materials can acquire important attributes such as narrow size distribution, core–shell processability, air stability, supramolecular assembly and intriguing optical, electronic, magnetic, chemical and biological phenomena.[16,17]

In this paper, we present a study in which the oxide shell of the core–shell particles $Au@ZrO_2$ and $Ag@ZrO_2$ has been modified with stearic acid ($CH_3(CH_2)_{16}COOH$). The first objective of the study was to increase the re-dispersibility of air-dried powders, especially in organic solvents. It should be noted that the parent materials, $Au@ZrO_2$ and $Ag@ZrO_2$, are dispersible only in highly polar solvents such as water and the air-dried powders are not re-dispersible. Purified monolayer covered particles have been studied using a variety of tools, principally focusing on the monolayer so as to compare and contrast it with that on metal nanoparticles, which was our second objective. Studies on monolayer protected metal nanoparticles have shown that the alkyl chains are all-*trans* and the extended chains form a pillar-like assembly on the crystal planes of the nanoparticle surfaces.[1e–g] This order, existing in longer chain monolayers (above a chain length of eight carbon atoms), collapses at the monolayer melting temperature above which the chains are dynamic.[18–20] The present studies show that the monolayer assemblies in these two core–shell systems are significantly different. We chose to study a coating of longer chain length as it is expected that the monolayer assembly would be more ordered. It is also expected that longer chain lengths would increase the temperature stability.

Experimental

Synthesis of core–shell nanomaterial

$HAuCl_4 \cdot 3H_2O$ was purchased from CDH chemicals and $AgNO_3$ was from Qualigens Chemicals. Zirconium(IV) propoxide and

† Electronic supplementary information (ESI) available: laser desorption mass spectrum, differential scanning calorimetric traces, and thermogravimetric analyses of the materials (3 pages). See http://www.rsc.org/suppdata/jm/b3/b313850j/

DOI: 10.1039/b313850j

stearic acid were from Aldrich and were used as received. All the solvents used in the synthesis were from local sources and were distilled prior to use. The chemicals were of 99.5% or better purity, which was not independently checked except using UV-visible absorption spectroscopy when necessary. The procedure for the one-pot synthesis and purification of core–shell nanoparticles of gold and silver with zirconia shells is reported in detail elsewhere.[5] Briefly, a solution containing equimolar (19.9 mM) amounts of zirconium(IV) propoxide and acetyl acetone in 2-propanol was prepared. A clear solution was formed upon mild sonication. Another solution of 8.80 mM $AgNO_3$ (or $HAuCl_4 \cdot 3H_2O$) and 13.88 M H_2O in DMF (dimethyl formamide) was prepared. 40 ml of the first solution and 20 ml of the second solution were mixed and stirred for about 10 minutes. The mixture was transferred to a heating mantle and refluxed for 45 minutes. The solution became pink in the case of Au and green-black in the case of Ag. For purification, the material was precipitated by slow addition of toluene, washed with 2-propanol and re-suspended back in 2-propanol.

Functionalization of the shell with stearic acid leading to Au/Ag@ZrO_2@stearic acid

To a 3 ml purified solution of Ag@ZrO_2/Au@ZrO_2, varying amounts (50 μl each) of 1% stearic acid solution in 2-propanol were added whilst stirring gently; the stirring was continued for 10 minutes to ensure complete adsorption. Adsorption of stearic acid was evidenced by the slow coagulation of the particles and the start of precipitation. It was often necessary to centrifuge the solution to achieve complete precipitation. The precipitate was washed with 2-propanol, cleaned and re-suspended back in 2-propanol (with sonication) to get a clear suspension; a dilute solution of which is stable for four months. (For XRD, NMR and DSC measurements, the reaction was carried out in bulk and excess stearic acid was removed by washing with 2-propanol.) The material could be re-precipitated by the addition of toluene. The precipitate was air dried and stored. No degradation was observed for a period of four months. The dry samples were pink in color for Au and greenish black for Ag. The material exhibited an –OH stretch in the infrared spectrum indicating that the surface is partly hydrated, which made it possible to disperse them in polar media as well. Oven drying resulted in a decrease in the –OH stretch intensity but the re-dispersibility was reduced. The material did not contain free stearic acid or any of the residues of the starting materials. The complete re-dispersibility of the powder in organic solvents demonstrated that ZrO_2 shells of the nanoparticles are coated with the stearate groups.

Characterization techniques

UV-visible spectra were recorded with a Perkin Elmer Lambda 25 spectrometer. Transmission electron microscopy (TEM) was performed with a Philips 120 keV TEM at the Indian Institute of Technology, Madras, India and with a JEOL 3010 high-resolution transmission electron microscope operated at 300 keV at the Technical University of Darmstadt, Germany. Samples for transmission electron microscopy were prepared by dropping a dispersion of the particles on copper grid supported Formvar films, carbon films or holey carbon films. Infrared spectra were measured using a Perkin Elmer Spectrum One spectrometer. All samples were prepared in the form of 1% (by weight) KBr pellets and all spectra were measured with a resolution of 4 cm^{-1}. Variable temperature IR measurements on KBr pellets were done with a home-built cell and a programmable temperature controller. Raman analyses were performed with a Bruker IFS 66v FT Raman spectrometer. X-Ray diffraction studies were carried out in a Shimadzu XD-D1 diffractometer with Cu Kα radiation (30 kV, 20 mA) at room temperature. The samples were spread on anti-reflection glass slides to give uniform films. The films were wetted with acetone for uniformity and were blow-dried before measurement. Differential scanning calorimetric (DSC) measurements were taken with a Netzsch PHOENIX DSC 204 instrument. About 10 mg of the sample encapsulated in aluminium pans were used. The measurements were conducted in the temperature range 20–200 °C in nitrogen atmosphere. A scan speed of 5 °C min^{-1} was used for the measurements. Thermogravimetric (TG) data were acquired with a Netzsch STA 409C instrument. Data in the range 20–1000 °C were measured in nitrogen atmosphere. A scan speed of 10 °C min^{-1} was used in these measurements. While air-dried samples were used for TG and DSC, samples dried at 100 °C were used for IR and XRD analyses. Nuclear Magnetic Resonance (NMR) spectra were measured with a JEOL GSX 400 MHz multi-nuclei FT-NMR spectrometer. Laser desorption mass spectra were taken with an Applied Biosystems Voyager DE PRO time of flight mass spectrometer.

Results and discussion

The colloids formed were characterized by UV-visible absorption spectroscopy. Au@ZrO_2 and Ag@ZrO_2 show characteristic surface plasmon absorption peaks at 526 and 428 nm, respectively.[5] The shift in the plasmon wavelength from bare nanoparticles (520 nm for gold and 400 nm for silver) is due to the dielectric cover surrounding the clusters.[21] This shift is explainable on the basis of the classical Mie's theory.[22] Fig. 1A shows the effect of addition of stearic acid on the absorption

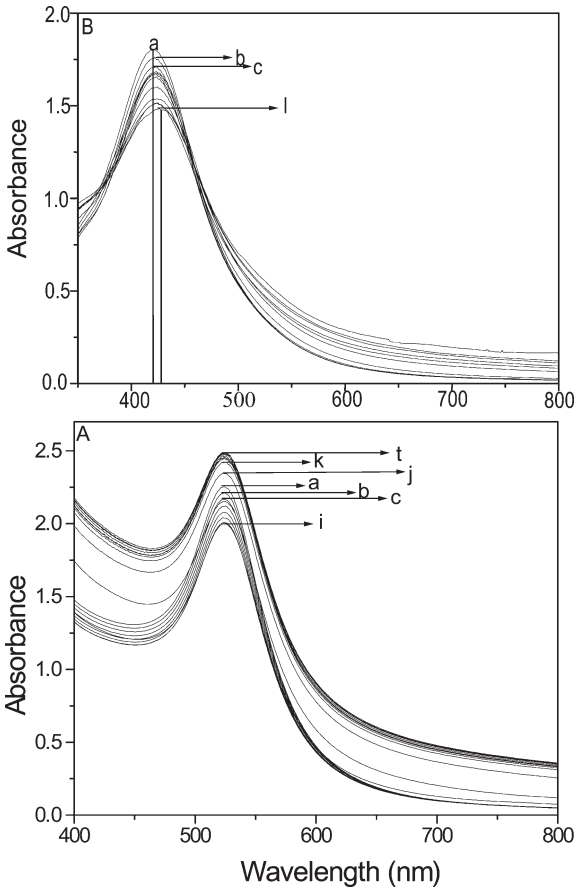

Fig. 1 (A) The effect of addition of stearic acid on Au@ZrO_2. Trace a is the absorption spectrum of pure Au@ZrO_2. Trace b was recorded just after the addition of 50 μl of stearic acid. Traces c–j are the UV-visible spectra corresponding to the further addition of 50 μl each. Traces k–t represent the time dependent spectra taken at every 10 minutes thereafter. (B) UV-visible spectra showing the corresponding sequences in Ag@ZrO_2.

spectrum of Au@ZrO_2. Trace a is the absorption spectrum of pure Au@ZrO_2 showing a plasmon absorption maximum at 526 nm. Trace b was recorded just after the addition of 50 μl of 1% stearic acid (in 2-propanol) to 3 ml of the cluster solution. The fact that the absorption spectrum remains the same without any shift confirms that the binding of stearic acid is confined to the ZrO_2 shell. With further addition of stearic acid in 50 μl quantities, the original plasmon shape is retained up until an added volume of stearic acid of 450 μl (c–i). During each addition, the absorbance decreases because of the dilution of the solution formed. When the volume of stearic acid became 500 μl (trace j), the absorbance is raised above that of trace a, and at this stage the solution shows signs of coagulation. This can be attributed to interlocking of the core–shell assembly through monolayers (as the alkyl chains have orientational freedom, see below) resulting in an increase in scattering, which increases the background in the spectrum. Further addition of stearic acid does not alter the monolayer coverage. The resulting solution was monitored in a time dependent manner, and the subsequent traces (k–t) were recorded at an interval of 10 minutes, thereafter gradual precipitation occurs. An identical reaction sequence was noted for Ag@ZrO_2 (Fig. 1B), but precipitation of the material begins after the addition of 350 μl of stearic acid itself, without any visible signs of coagulation. A shift of 10 nm is visible due to adsorption on the shell surface. This difference in the behaviour between Au and Ag samples is attributed to the decrease in the shell thickness for the latter. We have investigated particles with complete monolayer coverage only.

Fig. 2 shows a low magnification HRTEM image of several Ag@ZrO_2@stearate particles. The average particle size is of the order of 20 nm and the morphology is mostly near spherical. Similar results were seen for Au@ZrO_2@stearate particles. Fig. 3 shows HRTEM images of particles displaying core–shell morphologies. The shell region marked X in Fig. 3(a) is clearly crystalline showing fringes with a spacing of 2.5 Å which would correspond to the {110} or (002) planes of tetragonal ZrO_2. The shell areas marked Y and Z in Fig. 3(b) appears amorphous, although it could simply be crystalline ZrO_2 oriented such that no crystal lattice planes are oriented approximately parallel to the electron beam. It may be noted that the contrast of the shell against the strongly scattering silver core is fairly weak and sometimes difficult to distinguish from the carbon support film, especially for Fig. 3(b) where the shells do not display lattice fringes. This applies to an increased degree for Au@ZrO_2 as a result of the increased difference in average atomic number making it very difficult to obtain satisfactory images of the core-shell structure.

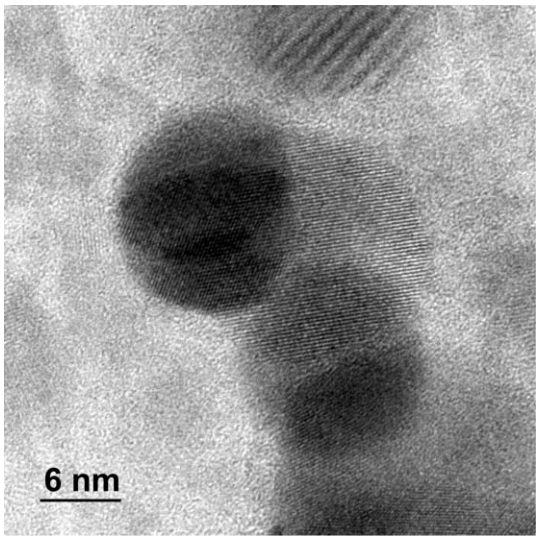

Fig. 2 HRTEM image of several (partially overlapping) Ag@ZrO_2@stearate particles. The average particle size is about 20 nm.

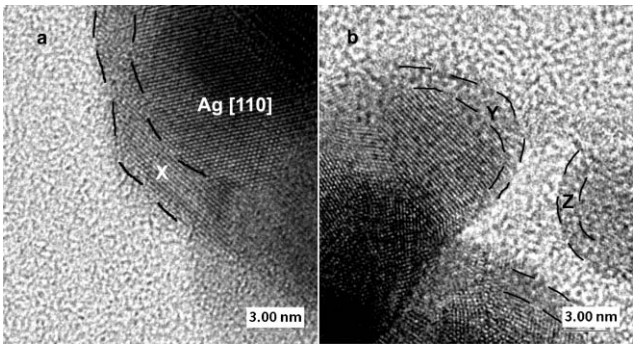

Fig. 3 HRTEM images of Ag@ZrO_2 particle edges: a) shows a crystalline shell on an Ag particle indicated with an X, the 2.5 Å spacing fits the (110) or (002) planes of tetragonal zirconia; b) shows apparently amorphous, or at least misaligned, shells on Ag particles (Y and Z).

XRD was performed on both the air-dried Au@ZrO_2@ stearate as well as on the powder dried at 600 °C for 5 hours (Fig. 4). In the air-dried sample (Fig. 4(a)); the core manifests peaks due to (111), (200) and (220) reflections corresponding to bulk fcc Au, as well as a broad ZrO_2 peak at around 31–32°. The peak widths correspond to an average crystallite size of about 7 nm for the Au as derived from the Scherrer formula. This may be easily rationalised with the TEM observations in

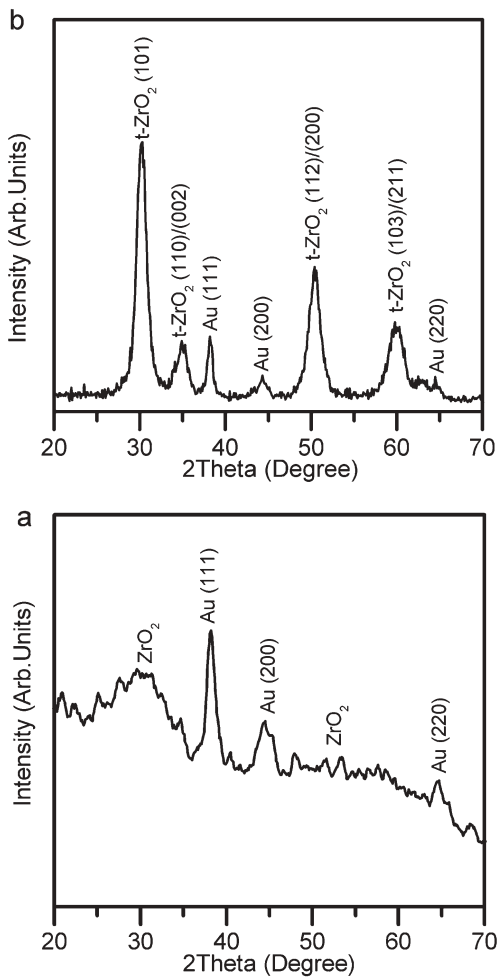

Fig. 4 XRD patterns of Au@ZrO_2@stearate powders; a) air-dried; and b) heat-treated at 600 °C for 5 hours. In the air-dried sample, the core manifests peaks due to (111), (200) and (220) reflections corresponding to bulk fcc Au. In the heated sample, a pattern containing sharper peaks from tetragonal zirconia and gold can be seen.

that many particles were observed to be polycrystalline. The breadth of the ZrO_2 peak and the noise in the signal make an exact measurement of crystallite size impossible, although it would seem to be less than 1 nm. It could well be that this is a mixture of amorphous and nanocrystalline zirconia, as seen in the TEM pictures. Upon heating the sample to 600 °C, a pattern containing much stronger and sharper peaks from zirconia, in addition to the gold peaks, is seen (Fig. 4(b)). The zirconia peaks are consistent with either the tetragonal or the cubic form. It may be noted in this connection that the normal room temperature monoclinic structure of zirconia has been shown to be suppressed at the very smallest particle sizes (<20 nm) and is then replaced by the tetragonal form.[23] The peak width of the ZrO_2 (101) peak would suggest a crystallite size of about 6.5 nm; the peak width of the gold (111) peak gives a crystallite size of ≈ 12 nm. This certainly suggests that significant crystal growth has taken place at 600 °C, especially as concerns the ZrO_2 shells, it may also suggest that neighboring particles have started to coalesce. The increase in gold crystallite size is less marked and is perhaps more likely to be related to the elimination of internal grain boundaries in the particles than to the direct coalescence of particles. Clarification of the exact behavior in the heat-treatment would require further TEM investigations, although it is already clear from these XRD experiments that the structures of the particles are being significantly changed.

Adsorption of stearic acid on the ZrO_2 shell was confirmed by infrared spectroscopy. Fig. 5(a) shows the IR spectrum of Au@ZrO_2@stearate. Fig. 5(b) is the IR spectrum of stearic acid showing the characteristic features[24] at 2921 cm^{-1} (C–H asymmetric stretching), 2851 cm^{-1} (C–H symmetric stretching), 1698 cm^{-1} (C=O of –COOH), 1472 cm^{-1} (–CH_2– deformation) and 1292 cm^{-1} (C–O symmetric stretching). Almost all the IR features of stearic acid broaden upon adsorption. Disappearance of the sharp band at 1700 cm^{-1} indicates that the carboxylic acid is in the form of –COO[25] and not –COOH and a monolayer of stearate is formed on the oxide surface. The emergence of a relatively intense infrared feature at 1521 cm^{-1} corresponds to the asymmetric carboxylate stretching of –COO, which again confirms the adsorption of stearic acid as stearate. This also rules out the possibility of multilayer adsorption of stearic acid. The peak at 653 cm^{-1} and a shoulder at 715 cm^{-1} may be attributed to IR active fundamental and longitudinal modes of ZrO_2.[26] In addition to the IR active features, additional peaks at 434 and 121 cm^{-1} were observed in Raman. The methylene peaks at 2921 (d_-) and 2851 (d_+) cm^{-1} suggest that the alkyl chains are conformationally disordered, like in the liquid state[18] For the solid-like all-*trans* conformation, the methylene peaks should appear at 2918 and 2846 cm^{-1}.[18] To further confirm the fact that stearic acid binds to the oxide surface in the form of stearate, a laser desorption mass spectrum of the air-dried Ag@ZrO_2@stearate precipitate was taken (ESI 1,† no matrix was used). The presence of a peak at $m/z = 283$ in the negative ion spectrum conclusively confirms the presence of stearate groups. Isotope patterns of Ag and ZrO_2 are clearly visible in the spectrum.

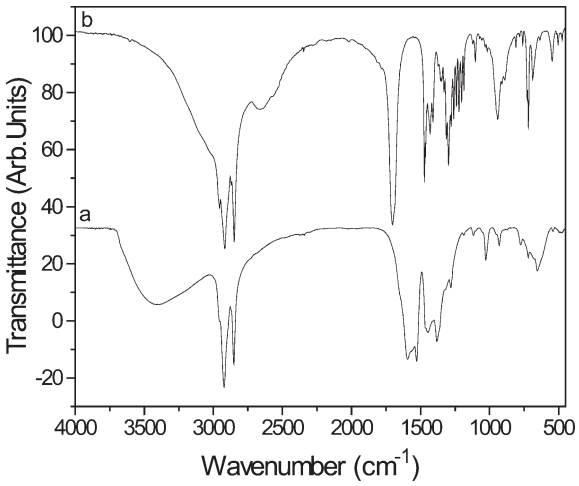

Fig. 5 IR spectra of (a) Au@ZrO_2@stearate and (b) pure stearic acid. Note that almost all the notable IR features of stearic acid were broadened and shifted due to adsorption on the shell surface, the most notable being the frequencies at 1648 and 1472 cm^{-1}.

We wanted to see whether there is any significant effect in the stearate layer with increase in temperature in a temperature dependent IR study. Fig. 6 shows the temperature dependent IR spectra of Au@ZrO_2@stearate in the temperature range of 25–225 °C at an interval of 25 °C (traces a–i). As can be seen, the only notable feature is the decrease of the –OH intensity with increase of temperature. There is no change in the position or intensity of the peaks of –CH_2 groups (symmetric and asymmetric stretching) implying that the stearic acid chains are in the molten state throughout. The symmetric and asymmetric CH_2 peaks show significant thermal broadening with temperature, which is also evident in the methyl modes. Only an irreversible loss of hydroxyl groups is happening in this temperature range and no desorption of stearic acid is observed. The sample was cooled to room temperature and the IR spectrum of the sample was again taken (trace j). The alkyl chain conformation remained in the disordered state. No exceptional change was noticed in IR after cooling. An identical observation has been noted in the case of Ag@ZrO_2@stearate as well. This confirms that the surface is principally hydroxylated and not hydrated; the latter would have resulted in a reversible absorption of water upon cooling.

The fact that alkyl chains are disordered is in stark contrast to the case of the monolayer chains on metal clusters (of Au and Ag), which exhibit an all-*trans* solid-like structure with the methylene peaks at the solid-like values.[1e,19,20] This conformational order is noted especially in the case of longer chains. The monolayers melt at higher temperatures and the melting temperature is related to the alkyl chain length.[1e,19,27] The fact that these features are distinctly different suggests that alkyl chains are adsorbed on the oxide surface and not on the metal, implying that the oxide cover is complete. We believe that the difference between the surface structure of the oxide and the

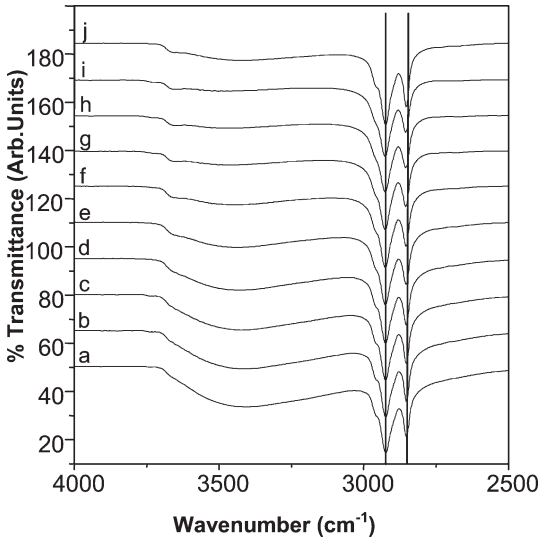

Fig. 6 Temperature dependent IR spectra of Au@ZrO_2@stearate. Trace a is the IR spectrum of the material at 25 °C. The subsequent traces (b–i) were recorded at 25 °C intervals up to 225 °C. Trace j is the IR spectrum after cooling the sample back to room temperature. Note that the only notable change is the loss of solvent in this temperature range. Lines at the d_+ and d_- positions are just a guide to the eye.

metal is the principal reason for the difference in the alkyl chain assembly. It is likely that some of the surface hydroxyl groups on the oxide surface have been functionalized by the acid, and as revealed by infrared spectroscopy, all the hydroxyl groups have not been covered. This means that there is sufficient room for the alkyl chains to exhibit mobility, making inter-chain van der Waals interactions negligible, unlike in the case of monolayers on metal clusters.[1e]

Differential scanning calorimetric traces (ESI 2†) of the solids show only one irreversible endotherm in the temperature range of 20–200 °C. The sample was first heated from 20 °C to 200 °C and then cooled back to 20 °C. The endotherm is attributed to the desorption of solvent or removal of surface hydroxyl groups in agreement with the IR spectra. DSC is irreversible as would be expected in the case of an irreversible change. Note that IR does not manifest an increase of hydroxyl peak intensity upon cooling. Thus the data are consistent with other studies.

The thermogravimetric analyses (ESI 3†) show gradual weight losses in the temperature range of 40–255 °C and a rapid loss in the range of 283–490 °C. The weight loss in the range of 40–255 °C is attributed to the loss of adsorbed solvent and surface hydroxyl groups whereas the subsequent loss is attributed to the desorption of the stearate groups (confirmed by infrared spectroscopy). Thus the data suggest the desorption of hydroxyl groups at higher temperatures.

Fig. 7 shows the ^{13}C NMR spectrum of Au@ZrO_2@stearate. The nearly dry precipitate of Au@ZrO_2@stearate was dispersed in D_2O for NMR analysis. The ^{13}C NMR signal of –COOH appears at 180.5 ppm in the case of free stearic acid dissolved in $CDCl_3$. In the case of Au@ZrO_2@stearate, the ^{13}C signal (signal 1) of –COO of bound stearic acid appears at 167.7 ppm. The absence of a ^{13}C peak around 180 ppm and the emergence of the same peak at 167.7 ppm can be attributed to the adsorption of –COOH groups. The peak is slightly broadened as compared to the parent molecule. The observation of this signal is attributed to the fact that the binding is on an oxide surface and not directly on the metal core, which could have broadened it to the baseline. The absence of –COOH proton was confirmed by ^1H-NMR spectroscopy. There are also some shifts in the ^{13}C signals of $-CH_2$ groups, which occur in the range of 22–34 ppm for free stearic acid. It is clear from the NMR spectrum that the carbons closest to the ZrO_2 shell interface (1–4 C of stearic acid) are broadened and appear below the peaks labeled 3 and 4.[27] The resonances narrow as the carbons are located far from the –COOH functionality. The NMR signal 2 can be attributed to C_{12}–C_{16}, signal 3 can be attributed to C_7–C_{10} and that labeled 4 can be due to C_5–C_6 of stearic acid, respectively. These assignments are along the lines of thiolate-protected nanoparticles.[27]

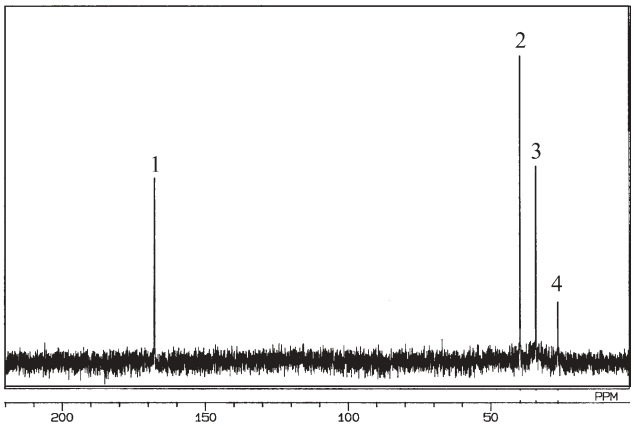

Fig. 7 The NMR spectrum of Au@ZrO_2@stearate. Note that the ^{13}C signal of the –COO of bound stearic acid appears at 167.7 ppm. The shift from the free ^{13}C value (180.5) is due to the binding of stearic acid on the ZrO_2 surface.

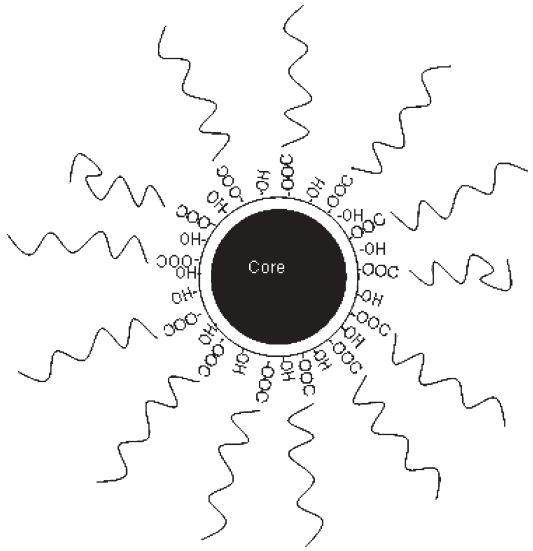

Fig. 8 The schematic view of the shell functionalised (Ag/Au)@ZrO_2@stearate core–shell nanocomposite. The core has a diameter of ~15 nm and the shell has a diameter of 3–4 nm. The zigzag chains in the figure correspond to the stearic acid chains. The presence of –OH groups in between the chains is to indicate the presence of surface bound hydroxyl groups on ZrO_2. The chains do not interact with each other making a liquid-like assembly. Some of the chains could even be bent.

On the basis of the data presented, an approximate structure of the functionalized core–shell particles is schematically represented in Fig. 8. The core of Au/Ag has a diameter of ~15 nm and the shell is of a typical diameter of 3–4 nm. The zigzag chains on the shell constitute the stearate units. The –OH groups in between represent the bound hydroxyl groups on the ZrO_2 surface. The chains do not interact with one another and, as a result, there is significant conformational disorder. Some of the chains could even be bent, as the disordered methylenes imply.[1e] Due to the high degree of mobility of the chains, the surface of the oxide shell is accessible for adsorbates. We have found that molecular adsorption on the ZrO_2 surface is possible for a variety of molecules; some of them penetrate the oxide shell and react with the metal core.[14] This is in agreement with the porous nature of the oxide shell. Disorder in the alkyl chains makes the particles interact in solution and this could lead to superlattice solids, if they are monodisperse.

Summary and conclusion

The surface modified Au@ZrO_2 and Ag@ZrO_2 core–shell materials were characterized by spectroscopic, microscopic, diffraction, and thermal analysis techniques. The re-dispersibility of the core–shell particles can be increased many-fold by the selective functionalization of the oxide shell using organic molecules. The air-dried samples are freely dispersible in a variety of organic solvents. The monolayers in these systems are distinctly different from those on metal nanoparticles and the chains are highly disordered implying widely spaced anchoring sites. As a result of this, the temperature dependent IR spectra are featureless, whereas the monolayers on metal nanoparticles show a distinct melting transition. As a result of the disorder in its structure, the monolayer permits absorbates onto the oxide surface. The oxide surface is partially hydroxylated even up to 200 °C. The monolayer anchoring is strong as desorption happens only above 280 °C. With the functionalization of the shell surface, these core–shell

nanosystems may acquire intriguing optical, electronic, magnetic, chemical and biological properties.

Acknowledgements

TP acknowledges financial support form the Space Technology Cell of Indian Institute of Technology Madras, and the Ministry of Information Technology for his oxide protected metal cluster research program. Mr. Thomas Utschig of Darmstadt University of Technology is acknowledged for his help in the initial stages of the TEM investigations. Prof. Dr. H. Fuess is gratefully acknowledged for the provision of the TEM facilities at the Darmstadt University of Technology.

References

1 (*a*) A. P. Alivisatos, *J. Phys. Chem.*, 1996, **100**, 13226; (*b*) O. V. Makarova, A. E. Ostafin, H. Miyoshi, J. R. Norris and D. Miesel, *J. Phys. Chem. B*, 1999, **103**, 9080; (*c*) C. J. Zhong and M. M. Maye, *Adv. Mater.*, 2001, **13**, 1507; (*d*) T. Ung, L. M. Liz-Marzan and M. Mulvaney, *J. Phys. Chem. B*, 1999, **103**, 6770; (*e*) N. Sandhyarani and T. Pradeep, *Int. Rev. Phys. Chem.*, 2003, **22**, 221; (*f*) T. Pradeep and N. Sandhyarani, *Pure Appl. Chem.*, 2002, **74**, 1593; (*g*) N. Sandhyarani, M. R. Resmi, R. Unnikrishnan, K. Vidyasagar, S. Ma, M. P. Antony, G. P. Selvam, V. Visalakshi, N. Chandrakumar, K. Pandian, Y.-T. Tao and T. Pradeep, *Chem. Mater.*, 2000, **12**, 104.

2 J. J. Schneider, *Adv. Mater.*, 2001, **13**, 529.

3 (*a*) S. Chen and R. W. Murray, *Langmuir*, 1999, **15**, 682; (*b*) K. Vijaya Sarathy, G. Raina, R. T. Yadav, G. U. Kulkarni and C. N. R. Rao, *J. Phys. Chem. B*, 1997, **101**, 9876.

4 (*a*) L. M. Liz-Marzan, M. Giersig and P. Mulvaney, *Langmuir*, 1996, **12**, 4329; (*b*) T. Li, J. Moon, A. A. Morrone, J. J. Mecholsky, D. R. Talham and J. H. Adair, *Langmuir*, 1999, **15**, 4328; (*c*) I. Pastoriza-Santos, D. S. Koktysh, A. A. Mamedov, M. Giersig, N. A. Kotov and L. M. Liz-Marzan, *Langmuir*, 2000, **16**, 2731.

5 R. T. Tom, A. Sreekumaran Nair, M. Aslam, A. Navinder, C. L. Nagendra, R. Philip, K. Vijayamohanan and T. Pradeep, *Langmuir*, 2003, **19**, 3439.

6 (*a*) B. O. Dabbousi, J. Rodriguez-Viejo, F. V. Mikulec, J. R. Heine, H. Mattoussi, R. Ober, K. F. Jensen and M. G. Bawendi, *J. Phys. Chem. B*, 1997, **101**, 9463; (*b*) M. Danek, K. F. Jensen, C. B. Murray and M. G. Bawendi, *Chem. Mater.*, 1996, **8**, 173; (*c*) X. G. Peng, A. V. Schlamp, A. V. Kadavanich and A. P. Alivisatos, *J. Am. Chem. Soc.*, 1997, **119**, 7019; (*d*) M. A. Hines and P. Guyot-Sionnest, *J. Phys. Chem.*, 1996, **100**, 468.

7 M. Bruchez, Jr, M. Moronne, P. Gin, S. Weiss and A. P. Alivisatos, *Science*, 1998, **281**, 2013.

8 W. C. W. Chan and S. Nie, *Science*, 1998, **281**, 2016.

9 (*a*) M. A. Correa-Duarte, M. Giersig and L. M. Liz-Marzan, *Chem. Phys. Lett.*, 1998, **286**, 497; (*b*) I. Pastoriza-Santos and L. M. Liz-Marzan, *Langmuir*, 1999, **15**, 948.

10 T. Ung, L. M. Liz-Marzan and P. Mulvaney, *J. Phys. Chem. B*, 1999, **103**, 6770.

11 F. Aliev, M. Correa-Duarte, A. A. Mamedov, J. W. Ostranger, M. Giersig, L. M. Liz-Marzan and N. A. Kotov, *Langmuir*, 2000, **16**, 2731.

12 (*a*) M. Hagelstein, H. O. Moser, D. Vollath, C. Ferrero and M. Borowski, *J. Synchroton Radiat.*, 2001, **8**, 522; (*b*) M. Forker, J. Schmidberger, D. V. Szabo and D. Vollath, *Phys. Rev. B*, 2000, **61**, 1014.

13 G. Christina and A. V. Blaaderen, *Langmuir*, 2002, **18**, 524.

14 A. Sreekumaran Nair, R. T. Tom, V. Suryanarayanan and T. Pradeep, *J. Mater. Chem.*, 2003, **13**, 297.

15 M. M. Y. Chen and A. Katz, *Langmuir*, 2002, **18**, 8566.

16 (*a*) M. Brust, M. Walker, D. Bethell, D. J. Schiffrin and R. Whyman, *J. Chem. Soc., Chem. Commun.*, 1994, 801; (*b*) D. I. Gittins, D. Bethell, D. J. Schiffrin and R. Nicholas, *Nature*, 2000, **408**, 67.

17 (*a*) A. C. Templeton, W. P. Wuelfing and R. W. Murray, *Acc. Chem. Res.*, 2000, **33**, 27; (*b*) J. J. Storhoff and C. Mirkin, *Chem. Rev.*, 1999, **99**, 1849; (*c*) A. N. Shipway, E. Katz and I. Willner, *ChemPhysChem*, 2000, **1**, 18; (*d*) L. Han, D. R. Daniel, M. M. Maye and C. J. Zhong, *Anal. Chem.*, 2001, **73**, 4441.

18 N. Sandhyarani, M. P. Antony, G. Panneer Selvam and T. Pradeep, *J. Chem. Phys.*, 2000, **113**, 9794.

19 S. Mitra, B. Nair, T. Pradeep, P. S. Goyal and R. Mukhopadhyay, *J. Phys. Chem. B*, 2002, **106**, 3960.

20 R. Mukhopadhyay, S. Mitra, T. Pradeep, T. Tsukushi and S. Ikeda, *J. Chem. Phys.*, 2003, **118**, 4614.

21 A. C. Templeton, J. J. Pietron, R. W. Murray and P. Mulvaney, *J. Phys. Chem. B*, 2000, **104**, 564.

22 G. Mie, *Ann. Phys.*, 1908, **25**, 377.

23 E. Djurado, P. Bouvier and G. Lucazeau, *J. Solid State Chem.*, 2000, **149**, 399.

24 N. L. Alpert, W. E. Keiser and H. A. Szymanski, *IR Theory and Practice of Infrared Spectroscopy*, Plenum Press, New York, 1963.

25 P. Antony and S. K. De, *Polymer*, 1999, **40**, 1487.

26 E. F. Lopez, V. S. Escribano, M. Panizza, M. M. Carnasciali and G. Busca, *J. Mater. Chem.*, 2001, **11**, 1891.

27 R. H. Terril, T. A. Postlethwaite, C. Chen, C.-D. Poon, A. Terzis, A. Chen, J. E. Hutchison, M. R. Clark, G. Wignall, J. D. Londono, R. Superfine, M. Falvo, C. S. Johnson, Jr., E. T. Samulski and R. W. Murray, *J. Am. Chem. Soc.*, 1995, **117**, 12537.